Role of zirconia phase transformation, interface processes, and Ta2O5 doping on the blistering phenomenon of molten glass in contact with zirconia-based refractories

J. Hell, P. Vespa, I. Cabodi, O. Citti, F. Fournet-Fayard, J. Fouletier, M.C. Steil

Role of zirconia phase transformation, interface processes and Ta_2O_5 doping on the blistering phenomenon of molten glass in contact with zirconia-based refractories

J. Hell[a, b], P. Vespa[a], I. Cabodi[a], O. Citti[a], F. Fournet-Fayard[b], J. Fouletier[b], M.C. Steil[b*]

[a] SEFPRO SGR Provence, F-84306 Cavaillon Cedex

[b] Univ. Grenoble Alpes, Univ. Savoie Mont Blanc, CNRS, Grenoble INP (Institute of Engineering and Management Univ. Grenoble Alpes), LEPMI, 38000 Grenoble, France

**Corresponding author*

Keywords:

blistering, molten glass, refractories, zirconia, doping

ABSTRACT

Bubble formation and removal within the molten glass is an important issue in glass industry. Various sources of bubbles have been identified in glass manufacturing: decomposition of the glass components, air trapping, oxidation/reduction reactions, precipitation resulting from insufficient refining, etc. It has been demonstrated in a previous paper that the blistering phenomenon at the interface between a molten glass and a zirconia-based refractory can be ascribed to the oxygen semipermeability through the zirconia phase. The objective of this study is to clarify the role of temperature on the blistering process, and especially, below and above the phase transition temperature of zirconia (monoclinic/tetragonal transformation) and to evaluate the role of zirconia doping on the blistering level. The influence of the kinetics of the surface processes at the glass/refractory interface is emphasized. Quantitative measurement of the slight blistering ascribed to the so-called "*redox shock*" is also given.

1. Introduction

The refractory linings in glass melting furnaces are in direct contact with the glass melt, and, consequently, have to suffer the aggressive conditions during liquid processing of glass. Two types of refractories are used, those synthesized by high-temperature electrofusion of precursor oxides, and those obtained by sintering of oxide powders. The first generation of fused-cast refractories, referred to as AZS (Al_2O_3 (ca. 45 wt.%) – ZrO_2 (ca. 35 wt.%) – SiO_2 (ca. 20 wt.%)) contains high amounts of alumina [1]. However, the necessity of producing high-purity glasses, i.e., crystal glass, glass ceramics, solar cells, television, smartphone screens, etc., led to the development of a second generation of refractory materials referred to as High Zirconia Fused-Cast refractories (HZFC) [2]. The room-temperature microstructure of HZFC refractories, consists of monoclinic zirconia (ca. 90 vol.%) embedded in a three-dimensional interconnected aluminosilicate glass (ca. 10 vol.%) [3].

During the fabrication of standard soda-lime-silica glasses, the melting of raw materials produces about 14 to 20 wt.% of carbon dioxide. Besides CO_2, several wt.% of water vapor are also released [4, 5]. The production of gases results from vaporization, decomposition and chemical reactions within the batch [6]. Glass refining is required to remove these gas bubbles from the glass melt. Sodium sulphate (Na_2SO_4) is the most used chemical fining agent in soda-lime glass industry. The refining process is an essential issue to obtain high-quality glasses. As an example, six bubbles per ton of glass leads to a 10 % rejection rate in television panel industry [7]. Insufficient fining can lead to a *reboil* phenomenon within the glass bulk, ascribed to sudden changes in temperature or in redox state [8, 9]. Moreover, bubbles can also be generated by the contact of refractory materials with glass melts. This effect referred to as blistering phenomenon has already been studied either with AZS (Al_2O_3 – ZrO_2 – SiO_2) fused-cast refractories [10, 11] or dense zircon ($ZrSiO_4$) [12, 13]. The formation of bubbles at the

refractory-glass interface has been also studied with ZrO_2-Al_2O_3 refractories melted either under reducing or oxidizing conditions [14, 15]. The composition of the bubbles was mainly CO_2 and SO_2 with reduced refractory, and O_2 and N_2 with oxidized one, respectively. The mechanism proposed was the reduction of sulfur trioxide dissolved in the glass by iron or carbon impurities of the refractory forming sulfur and carbon dioxides, respectively. In case of oxidized refractory, the formation of bubbles would result from entry in the glass of air enclosed in the porosity of the refractory. We have demonstrated in a previous paper [16], for the first time, that the blistering phenomenon with oxidized HZFC refractories, at temperatures below 1150°C, is ascribed to oxygen semipermeation through the zirconia phase. The role of oxidation state of the ceramic on the blistering phenomenon has also been emphasized. It has also been shown that, in case of monoclinic zirconia, which is a mixed ionic-electronic conductor, the permeation flux is controlled by the minority carriers that are ionic defects (either oxygen interstitials, O_i'', or oxygen vacancies, $V_O^{\bullet\bullet}$).

The aim of this paper was, first, to study the role of temperature, and of the phase transformation of zirconia on the blistering level and, second, to evaluate the role on the blistering process of doping zirconia with pentavalent oxides, such as Ta_2O_5. Using the set-up dedicated to the study of the blistering phenomenon, we also evaluated the slight blistering resulting from the so-called "redox shock".

2. Electrical transport in zirconia and blistering mechanism

There are three polymorphs for zirconia with two crystallographic transformations, i.e., monoclinic/tetragonal at ca. 1150°C and tetragonal/cubic at ca. 2375°C [17]. The temperatures of transformation depend on the particle size, stress, thermal history and impurities level. The monoclinic/tetragonal transformation has been studied using various techniques (X-Ray and electron diffraction, microscopy, differential thermal analysis (DTA), thermogravimetry,

electrical conductivity, spectroscopy, mechanical characterization, etc.), and reviewed by Subbarao [18, 19]. More recently, the transformation has been studied using Density Functional Theory Analysis [20, 21].

The electrical properties of pure zirconia have been studied since the beginning of the seventies [22–24]. However, there are disagreements in the published data, considering the methods of sample synthesis, their microstructure, the level of impurities, the thermal history of the sample, the techniques used for the electrical characterization, etc. It should be pointed out that the presence of foreign cations in the form of impurities significantly modifies the concentration of intrinsic defects [25, 26]. However, the intrinsic defect structure is approached as temperature increases [27]. It is also difficult to obtain dense, crack-free ZrO_2 because of the ca. 5 % volume change associated with the monoclinic/tetragonal transformation [28]. However, pellets prepared by vacuum hot-pressing [23], or using nanosized powders [29] exhibit densities higher than 90 % of the theoretical one.

The electrical conductivity has been measured using dc current [22], at constant frequency (ca. 10^4 Hz) [23, 27, 30], or in the frequency range 20 Hz to 20 kHz [23]. It has been shown that, at temperatures higher than 1000°C, the conductivity is frequency independent. The ionic and electronic contributions from the total electrical conductivity have been generally determined using electromotive force measurements using oxygen activity gradient cell [27, 30, 31]. It should be pointed out that the emf method is often not appropriate for determination of electronic transport numbers higher than one percent [32]. The Patterson method [33, 34] may be preferred; however, the knowledge of the ionic conductivity is required, that is generally not possible with pure zirconia because the ionic conductivity is controlled by impurities, mainly at low temperature [27]. At low temperatures, the grain boundary contribution is important, but disappears at high temperature [27, 35].

Various defect models have been proposed; the most recent experimental or theoretical works are consistent with the anti-Frenkel structure proposed initially by Douglas and Wagner [36], according to (using Kröger-Vink notation):

$$O_O^{\times} = O_i^{''} + V_O^{\bullet\bullet} \quad (1)$$

It has been demonstrated that the monoclinic phase is a mixed ionic-electronic conductor, with predominant electronic conductivity [23, 37]. On the contrary, the tetragonal phase is an ionic conductor [22, 24]. A noticeable increase of the electrical conductivity is observed at the monoclinic/tetragonal transition. This transition is martensitic in nature, with contraction on heating (5 vol. %) and a corresponding expansion on cooling [38]. The transformation exhibits a large thermal hysteresis. The forward transition occurs at 1170°C and the reverse one between 850° and 1000°C, depending on grain sizes, thermal history, etc. [19, 39]. It is accomplished by a diffusionless mechanism in which some of the atoms move by distances lower than one interatomic distance while other atoms nearly retain their original positions. The increase of the ionic conductivity can be ascribed to the high mobility of oxygen in the tetragonal structure [40, 41]. Tetragonal zirconia is obtained after 1150°C, but it can be obtained at much lower temperatures by stresses, doping or reducing the crystallite size [42, 43].

The equilibrium with the oxygen partial pressure can be written:

$$\frac{1}{2} O_2 + V_O^{\bullet\bullet} = O_O^{\times} + 2\,h^{\bullet} \quad (2)$$

or

$$\frac{1}{2} O_2 = O_i^{''} + 2\,h^{\bullet} \quad (3)$$

For pure zirconia, under high oxygen pressure the defects concentrations, both oxygen interstitials and electron holes increase with oxygen partial pressure. The ionic conductivity can be modulated by doping with oxides, either a dopant with a valence lower than 4 (such as CaO or Y_2O_3) or a dopant with a valence higher than 4 (such as Ta_2O_5) [44].

Doping pure zirconia with an oxide exhibiting a valence higher than 4, such as Ta_2O_5, induces a lowering in oxygen vacancy concentration, according to:

$$Ta_2O_5 + V_O^{\bullet\bullet} = 2\,Ta_{Zr}^{\bullet} + 5\,O_O^X \quad (4)$$

Consequently, the ionic conductivity decreases significantly. The following experimental results demonstrate the role of both the zirconia phase transformation and zirconia doping with Ta_2O_5 on the blistering phenomenon.

The blistering phenomenon involves various steps including bulk transport across the refractory and interface reactions. If we consider a HZC membrane, with air on one side and an inert gas on the other side, without molten glass, owing to the mixed ionic-electronic conductivity an oxygen transfer through the membrane is observed from the oxygen-rich side to the lean one [16]. A simplified mechanism of the oxygen permeation process involves three main steps, using Kröger-Vink notation [45-48]:

- Oxygen reduction and incorporation in the refractory at the external oxygen-rich side:

$$\frac{1}{2}\,O_2 + V_O^{\bullet\bullet} + 2\,e' = O_O^{\times} \quad (5)$$

- Bulk diffusion of oxygen vacancies and electronic defect within the zirconia phase of the refractory wall,
- Oxide ions oxidation and formation of oxygen at the glass/refractory interface:

$$O_O^{\times} = \frac{1}{2}\,O_2 + V_O^{\bullet\bullet} + 2\,e' \quad (6)$$

If one of these steps has finite kinetic constants and all other kinetic constants have infinite values, we deal with what is called a pure regime [49]. All the steps other than the limiting one equilibrate and the overall rate, common for all the steps, is fixed by the limiting one. As an example, in case of a permeation process limited by bulk diffusion, all the interface steps are at equilibrium and the blistering level is determined by the ambipolar conductivity value and the oxygen activity gradient across the membrane [16]. On the opposite, in case of the overall reaction rate is limited by an interface process, the ionic and electronic concentration gradients within the refractory wall are zero, the concentrations are constant in the refractory, and there

is no electric field in the refractory layer. Consequently, in case of air atmosphere outside the container, the oxygen activity at the interface Argon/refractory will be close to 0.2, and the permeation level will be very low.

In a previous publication we have studied the oxygen permeation process through HZC refractory, with the configuration air/HZC refractory/Argon [16]. In Figure 1 (a) the ideal situation is illustrated: both surfaces of the membrane are in equilibrium with the gas phase (hypothesis of Wagner) and the permeation flux depends on the bulk properties of the refractory, i.e., the oxygen flux depends on the ambipolar conductivity and on the oxygen gradient across the membrane. However, as reported in [16], the oxygen permeation flux was negligible, demonstrating that, with HZC refractory, the oxygen permeation process is controlled by interface reactions on the lean side of the membrane. The increase of the oxygen activity in the surface layer on the lean side induces a noticeable lowering of the oxygen activity gradient across the membrane and, consequently, the permeation flux will be very small (see Figure 1 (b)). This behavior has been observed previously with BIMEVOX solid electrolyte [50].

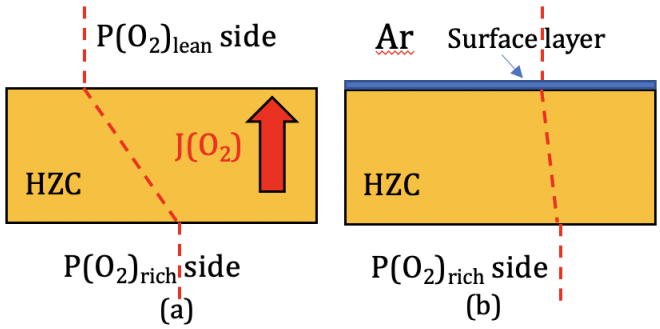

Figure 1: Illustration of the oxygen permeation process, (a): ideal case, (b): surface limiting process.

Obviously, in case of a mixed regime, the rate of the overall process is limited by more than one step.

Considering the blistering phenomenon, additional steps have to be considered, i.e., oxygen dissolution in the molten glass up to saturation, followed by nucleation, growth and detachment

of bubbles. Obviously, these steps depend on glass composition, glass impurities and on temperature. As an example, the oxygen solubility in a molten glass decreases noticeably as temperature increases. As shown in a previous paper, the time necessary for a bubble to be formed, rises in the glass melt and burst is of the order of 1 hour/cm of molten glass at about 1100°C [16].

3. Experimental

3.1.Studied materials

High-zirconia fused-cast refractories are obtained by electrofusion: the raw materials are melted at about 2500°C with electric energy created between graphite electrodes. The studied fused-cast product contains 91 wt.% ZrO_2 and 9 wt.% of a vitreous phase composed of SiO_2, Al_2O_3, Na_2O and B_2O_3. The tested AKM glass contains alkaline oxides ($Na_2O + K_2O$ ~ 15–22 wt.%), alkali-earth oxides (MgO + CaO > 5 wt.%) and also alumina (Al_2O_3 > 8 wt.%). The refractories were referred to as HZC and HZX (with ca. 1 wt.% Ta_2O_5), exhibiting a vitreous phase including 7 wt.% B_2O_3.

3.2. Electrical conductivity measurements

The electrical properties of the refractories were characterized by impedance spectroscopy. Conductivity measurements were carried out up to 1500°C. The sample holder, in alumina, can hold three samples, allowing simultaneous measurements in the same conditions. The samples were pre-treated at 1350°C for 30 hours under air. Both surfaces were coated with Pt paste (Pt ink 6926, Metalor), dried at 100°C and fired at 1000 °C for 2 hours. The gas flowing the cell was pure oxygen, synthetic air, argon, or argon-hydrogen (5%), with a flow rate of 6 L/h. The atmosphere around the samples was controlled and monitored using a laboratory-made zirconia pump-sensor device. Data acquisition was carried out by a 1260

Solartron frequency analyser in the 0.1 – 10^7 Hz frequency range. All measurements were normalized by the geometric factor $k = L/S$ (L: thickness of the sample, S: surface area of the pellets). The standard size of the samples used is a cylinder of 8 mm of diameter and 6 mm of thickness.

3.3. Self-crucible tests

Blistering tests were also carried out in self-crucible of HZC refractory (50 mm in external diameter, 30 mm in height, with wall thickness of 10 mm), filled with glass and heated, at 1100°C, and 1350°C for 30 h. and 200 h., under air. The crucibles were then cut transversely to form a slice 8 mm thick. Photos were taken and a bubble count performed to evaluate the role of temperature on the blistering, below and above the temperature of the monoclinic/tetragonal transformation.

3.4. In-situ blistering measurements

The set-up has been described in a previous paper [16]. As schematized in Figure 2, the studied refractory, sometimes pre-treated at 1350°C for 30 hours, was machined in the form of a crucible (external diameter: 19 mm, wall thickness: 3 mm, and 10 mm height), and inserted in the set-up. A solid glass pellet was introduced in the crucible before heating the cell (10 mm in diameter, around 1 mm thick). Nominally pure argon ($P_1 < 10^{-6}$ bar) was flowing in the upper part of the crucible, in contact with molten glass, at a 6 L/h flowrate. The gas-tightness was achieved by platinum O-rings. This cell was placed inside another alumina tube to create a guard-chamber with argon flow in order to limit the impact of eventual leakages. The atmosphere below the crucible was synthetic air ($P_3 = 0.2$ bar).

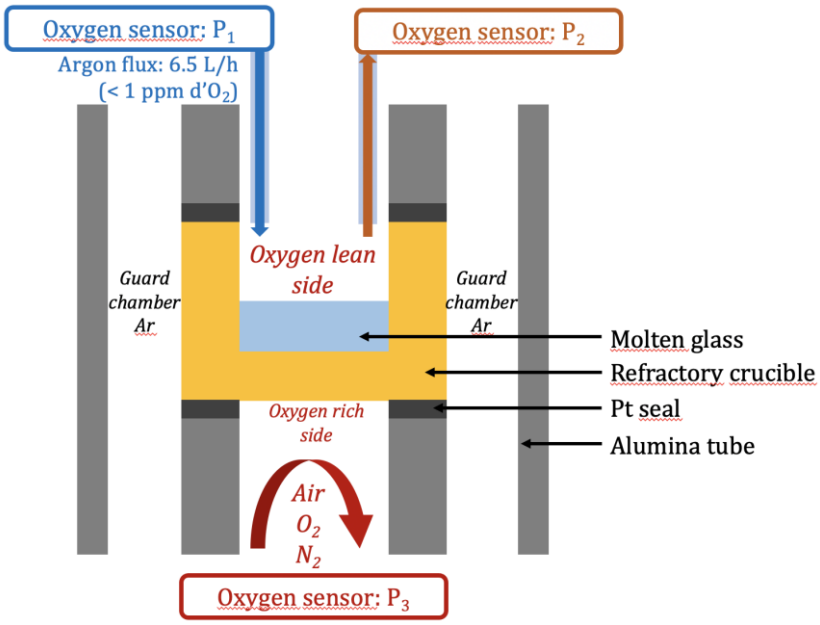

Figure 2: Semi-permeability set-up to study the blistering process in a glass in contact with a refractory, from [16].

The procedure was the following: heat at 100°C/h, from ambient temperature up to 1100°C, then a temperature plateau at 1100°C for 20 h, a second heating at 100°C/h up to 1350°C, with a plateau at this temperature for 5 h.

Laboratory-made zirconia sensors (reference: air) referred to as P_1, and P_2 were used for measuring the oxygen partial pressure upstream, and downstream the cell, respectively. The emf, E, of the zirconia sensor (P_2), downstream the cell was recorded continuously (data acquisition every second), and shows various peaks (Figure 3 (a)). Each peak corresponds to one (or several) oxygen bubble(s) exploding on the surface of the molten glass and increasing the oxygen concentration in the flowing gas. According to the Nernst law, the oxygen mole fraction, x_2, in the flowing gas, can be calculated from:

$$x_2 = 0.2 \times 10^{20183 \times E/T} \quad (7)$$

where E is in V., and T is the sensor temperature, in K. As an example, for E = - 0.15 V, at 700°C, the oxygen mole fraction is 1.55 x 10^{-4} (often referred to as 155 ppm). If D is the argon gas flowrate, the oxygen flux can be calculated (see Figure 3 (b)):

$$v_{O_2} = x_2 \times D \quad (8)$$

It should be pointed out that the basis line in Figure 3 (a) corresponded always to an oxygen content lower than 10 ppm indicating the high gas-tightness of the set-up.

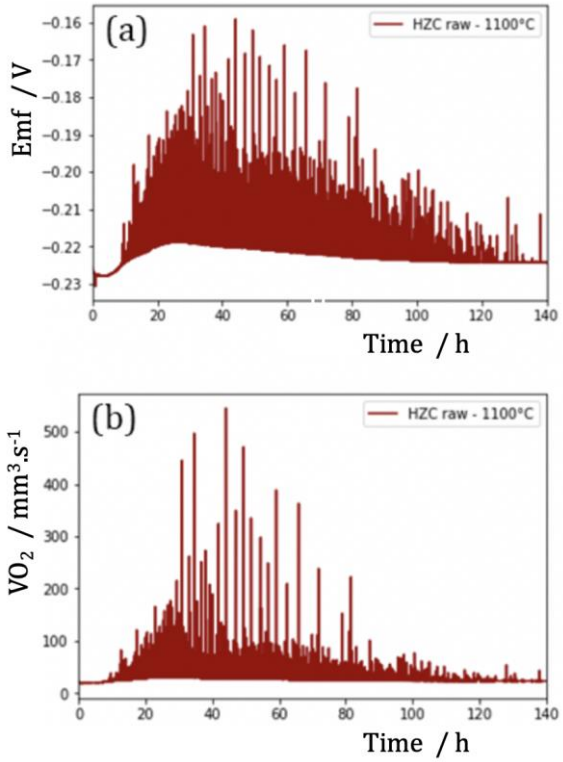

Figure 3: Data treatment of the sensor emf: (a) sensor emf vs. time, (b) oxygen flux, in $mm^3.s^{-1}$. Blistering experiments with AKM glass in contact with a HZC refractory (pO_2 (3) = 0.2 bar), at 1100°C.

4. Results and discussion

4.1. Electrical transport

Figure 4 shows the evolution of the impedance diagrams as a function of the measuring temperature obtained for the HZC refractory, under air, in the 700–1200°C range. The Nyquist diagram of the sample recorded at 700°C with the respective fitting results are given in Figure 4 (a). The spectra are composed of three depressed semicircles. The high frequency one, referred to as "Bulk", is the characteristic response of the matrix. In the case of homogenous and dense ceramics, it is quasi-identical to that of a single crystal of the same

composition and the medium frequency semicircle ("Blocking") describes the blocking contribution. The medium frequency contribution can be related to the zirconia/vitreous phase interface, or to zirconia/zirconia grains contacts. In addition, the low frequency semicircle ($f < 10^3$ Hz) corresponds to the electrode response. The deconvolution of the material response into two contributions, i.e., bulk and blocking, were easy at low temperature (Figure 4 (a)). As illustrated by Figures 4 (a) to (d), the higher the temperature, the smaller the grain boundary contribution. At temperatures higher than 850°C, the grain boundary contribution becomes negligible, and, consequently, the high frequency contribution can be ascribed to the material property (R_{tot}). A shift towards the high frequencies of the observed responses can be observed when temperature increases. At 1200°C, the high frequency region of the diagram is modified by inductive effects of the set-up. However, as shown previously [16], it should be pointed out that the refractory is a heterogeneous material constituted by zirconia grains and a vitreous phase, and it has been demonstrated that the bulk response results from a combination of the electrical properties of the two phases contained in the material, i.e., the semi-circle corresponding to the bulk is the overall electrical properties of the conductive matrix modified by the presence of a second phase [51–53]. Consequently, only an apparent zirconia conductivity (σ_{app}) can be obtained. However, in case of poor conductivity of the minority vitreous phase (less than 10 wt. %), the electrical behaviour of the refractory can be ascribed mainly to the zirconia phase.

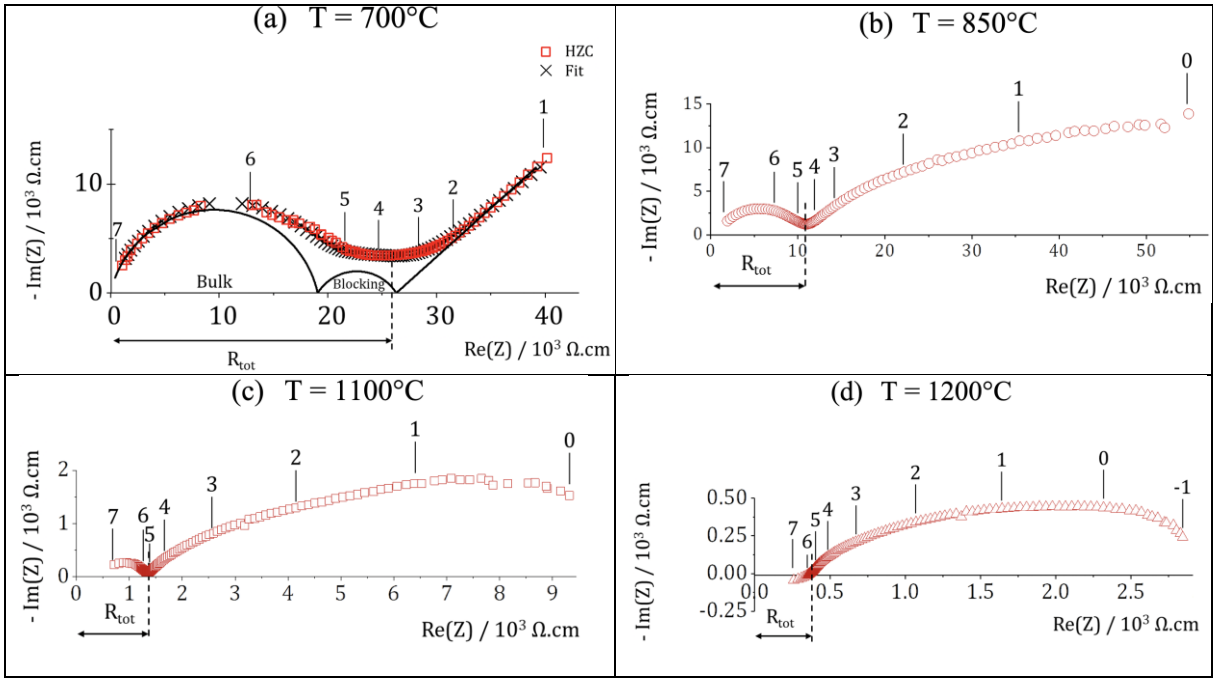

Figure 4: Normalized impedance diagrams of HZC refractory, under air atmosphere (pO_2 = 0.2 bar) at (a) 700 °C, (b) 850°C, (c) 1100°C, and (d) 1200°C. R_{tot} is estimated with an error of 5%. (The numbers 1, 2, etc. indicate the logarithms of the measuring frequencies in Hz). The fitting result in Figure 4 (a) is shown as a solid black line.

Figure 5 shows Arrhenius plots of the total electrical conductivity σ of the studied samples, with increasing temperatures. Three domains are evidenced that can be related to the crystalline phase changes of zirconia: monoclinic phase at low temperatures, phase transition and tetragonal phase at high temperatures. The phase transition is clearly observed around 1150°C. It should be pointed out, by heating temperature measurements, that the transition temperature of the tested refractories coincides with the results obtained by Vest et al. [24] with pure zirconia.

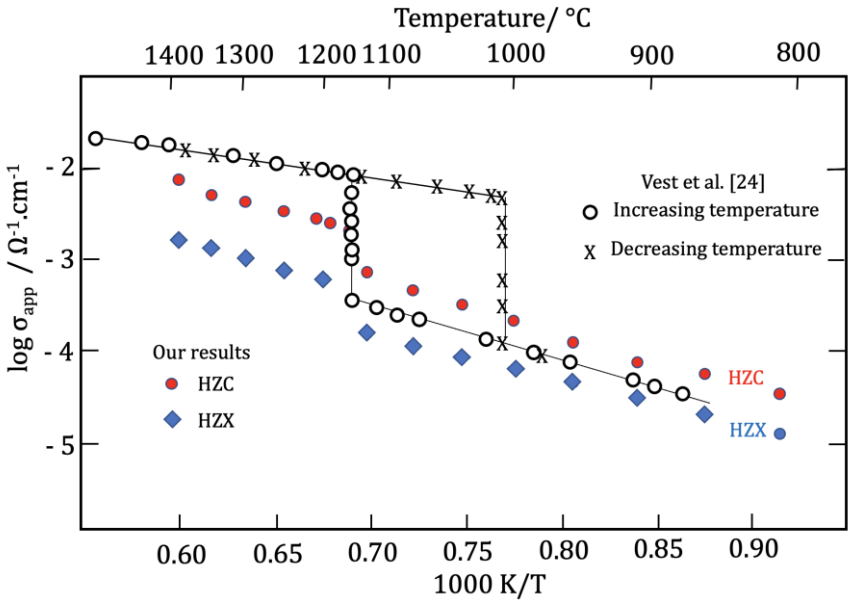

Figure 5: Arrhenius plot of HZC and HZX refractories, between 550°C and 1450°C (heating), under air atmosphere, with platinum electrodes. The results obtained by Vest et al. [24] with pure zirconia are plotted for comparison.

Above the transition temperature, the conductivity of the HZX refractory is a power of ten lower than pure tetragonal zirconia which is an ionic conductor, due to lowering of the intrinsic oxygen vacancies concentration by Ta_2O_5 doping (see equation (4)).

The calculated activation energy values are shown in Table 1. Kwon et al. [29] have compared the previously published activation energy of the electrical conductivity of monoclinic and tetragonal zirconia. As recalled in Section 2, the conductivity results are very scattered. However, our results agree well with those obtained by Muccillo et al. with highly pure zirconia [39], i.e., 0.9 eV and 1.1 eV, respectively, for the tetragonal and monoclinic phases.

Table 1: Activation energy, E_a, of the electrical conductivity below and above the transition temperature, under air.

Reference	E_a /eV below 1150°C	E_a / kJ.mol^{-1} below 1150°C	E_a /eV above 1150°C	E_a / kJ.mol^{-1} above 1150°C
HZC	1.1	106	1.1	106
HZX	1.1	106	0.9	87

The variation of the electrical conductivity of the HZC refractory as function of the oxygen partial pressure, referred to as a Patterson diagram, at 1100°C, is given Figure 6. The monoclinic phase was obtained on the first heating of the sample. The tetragonal phase was obtained after first heating at 1400°C, cooled at 1100°C after that, which is noticeably above the tetragonal/monoclinic transformation under cooling. Below ca. 10^{-5} bar, a conductivity plateau was observed for both samples indicating a pure ionic conductivity, which is fixed by intrinsic defects and impurities of the sample. The apparent ionic conductivity of the tetragonal phase is ca. 2 times higher than that of the monoclinic one, owing to a higher mobility of the oxygen vacancies. Under air, as expected, the apparent electronic transport number of monoclinic HZC is noticeably higher than that of the tetragonal phase, i.e., 0.68 and 0.46, respectively.

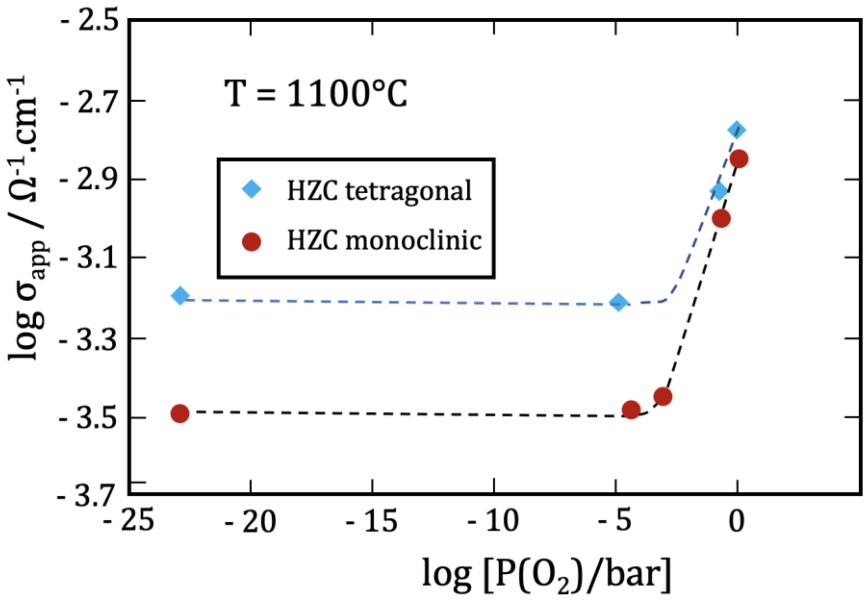

Figure 6: Variation of the electrical conductivity with oxygen partial pressure of monoclinic and tetragonal HZC refractory, at 1100°C.

Figures 7 (a) and (b) compare the variations of the apparent electrical conductivity of HZC and HZX refractories as a function of the oxygen partial pressure, at 1100°C and 1200°C.

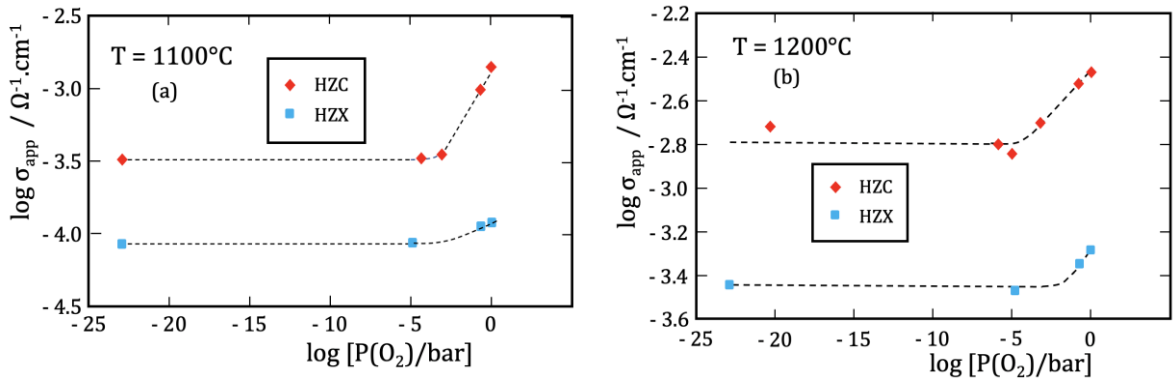

Figure 7: Patterson diagrams at 1100°C (a) and 1200°C (b) for HZC and HZX. (The lines are only a guide for the eye).

The same shape is observed for all the refractories below and above the monoclinic/tetragonal transformation of zirconia with a plateau in the low oxygen pressure range and an additional p-type electronic conductivity under high oxygen partial pressures. Even if, as expected, the apparent ionic conductivity of HZX is lower than that of HZC, owing to the Ta_2O_5 doping, it should be recalled, as shown in a previous publication [16], that the vitreous phase modulates the conductivity of the zirconia phase. The lower the conductivity of the vitreous phase, the lower the difference between the measured apparent conductivity and the actual conductivity of the zirconia phase. The vitreous phase in both studied refractories including ca. 7 wt.% of B_2O_3 is insulating, consequently, as recalled previously, the electrical behaviour of the HZC refractory approaches the one of zirconia and the conductivity increase at high oxygen partial pressure can be ascribed mainly to the additional p-type conductivity.

According to Wagner's theory, assuming that bulk diffusion within the refractory is the rate limiting process, the oxygen semipermeation flux is proportional to the ambipolar conductivity σ_{amb}, with $\sigma_{amb} = \sigma_i \sigma_e/(\sigma_i + \sigma_e)$. From the apparent ionic and electronic conductivities obtained using Figure 7, the resulting apparent ambipolar conductivity was evaluated. For the HZC refractory, the ambipolar conductivity was, respectively, 2.4 x 10^{-4} $\Omega^{-1}.cm^{-1}$ and 1100°C, and

$8.4 \times 10^{-4}\ \Omega^{-1}.cm^{-1}$, at 1200°C, indicating an increase of the ambipolar conductivity beyond the monoclinic/tetragonal transformation.

4.2 Redox shock and thermal reboil

Glass may contain impurities or additives introduced during the glass fabrication which exist in more than one oxidation state, such as iron, copper, antimony or sulphate ions. The blistering phenomenon at high temperature has been ascribed in the literature to an electrochemical reaction between the glass and the refractory and is referred to as a "*redox shock*" between the refractory and the glass. This phenomenon results from a significant difference in redox state between the glass and the vitreous phase of the refractory. As an example, as demonstrated in a previous publication [16], a raw refractory contains some metallic iron that can react with sodium sulphate used in the fining process: sodium sulphate may be reduced to form SO_2 bubbles, with exhibit a low solubility in glass, according to the following reaction:

$$Na_2SO_{4,glass} + Fe_{refractory} \rightarrow SO_{2,glass} + FeO_{refractory} + Na_2O_{glass} \qquad (9)$$

Formation of bubbles within the glass can also be ascribed to the thermal "*reboil*" phenomenon, which is the formation of bubbles in supersaturated glass when heated to a high temperature [54]. This phenomenon may be observed in case of reheating glasses. Gases for which there is an increase in solubility with increasing temperature do not contribute to reboil, since supersaturation occurs because the solubility of the dissolved gas is lower at the higher temperature. Krämer [55] has reviewed the solubility of various gases in molten glasses. The solubility of SO_3 and CO_2 decreases as the temperature increases. Consequently, if bubbles of SO_3 remain in the molten glass after the refining process, increasing solubility at lower temperature will lead to their dissolution during the cooling process. However, the solubility of

SO_3 in commercial soda-lime-silicate melts decreases by three orders of magnitude on heating from 1000 to 1400°C. Under these conditions, a small increase in temperature can convert a previously plain unsaturated melt into a highly supersaturated one, which induces formation of bubbles. Some glasses are much more inclined than others to show this instability, which depends on glass composition, redox state, etc.

The fining process for the tested glasses was carried out using sodium sulphate (Na_2SO_4), consequently, the gases that could evolve according to redox shock or reboil phenomena are mainly oxygen and sulfur dioxide. The gases that eventually evolve were analysed by coupling the semipermeability set-up (Figure 2) with a mass-spectrometer for analysing simultaneously O_2 and SO_2. To avoid a blistering phenomenon due to the presence of oxygen, the three chambers of the set-up (see Figure 2), were flushed with pure argon. Consequently, in case of redox shock process, the gas that could evolve is mainly sulphur dioxide. Figures 8 and 9 compare the SO_2 and O_2 levels, for a raw HZC refractory in contact with AKM glass under argon atmosphere ($pO_2 = 10^{-5}$ bar), at 1250°C. About 20 peaks ascribed to SO_2 were observed during the first 20 minutes and no peaks corresponding to oxygen. As shown in a previous publication [16], the mass spectrometry intensity for oxygen corresponds to an oxygen content in the flowing argon lower than 10 ppm.

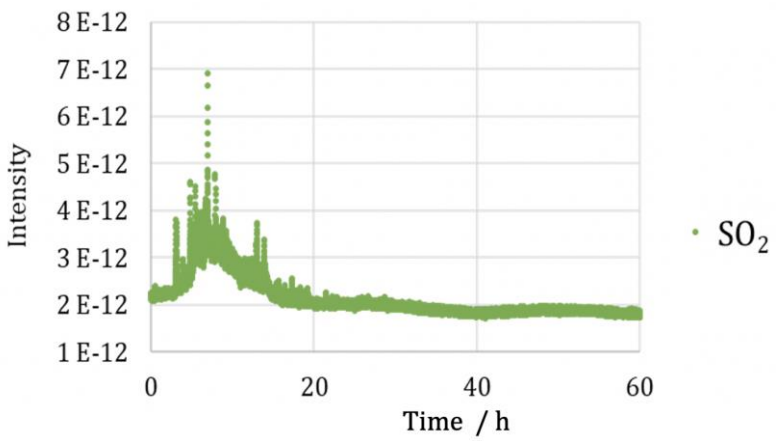

Figure 8: Mass spectrometry analysis of SO_2: AKM glass in contact with a raw HZC refractory at 1250°C under argon atmosphere.

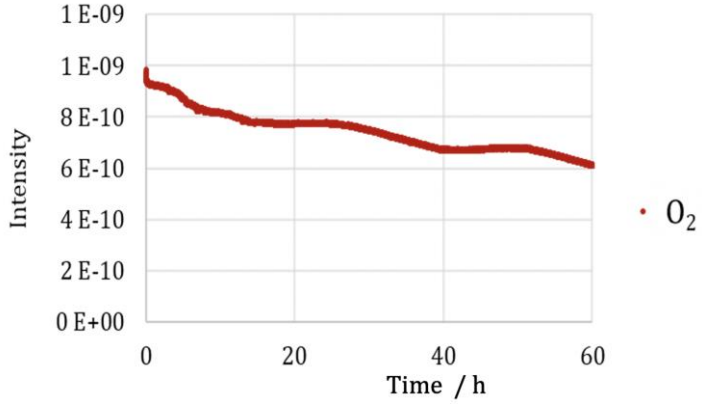

Figure 9: Mass spectrometry analysis of O_2: AKM glass in contact with a raw HZC refractory at 1250°C under argon atmosphere.

It should be noted that, in agreement with equation (9), the redox shock was observed only with raw refractories, containing metallic iron impurities. Figure 10 compares the mass spectrometer signals obtained for SO_2 (Figure 8), with the blistering phenomenon observed, at 1100°C with air outside the HZC crucible. It should be noted that the oxygen flux is more than 1000 times higher than the SO_2 blistering. Moreover, a continuous and intense O_2 blistering was observed while only few SO_2 peaks were observed during the first 20 minutes of the test (Figure 8). With

oxidized refractory, no SO_2 was detected, indicating that the blistering can be ascribed to a *redox shock* and not to a *reboil* phenomenon.

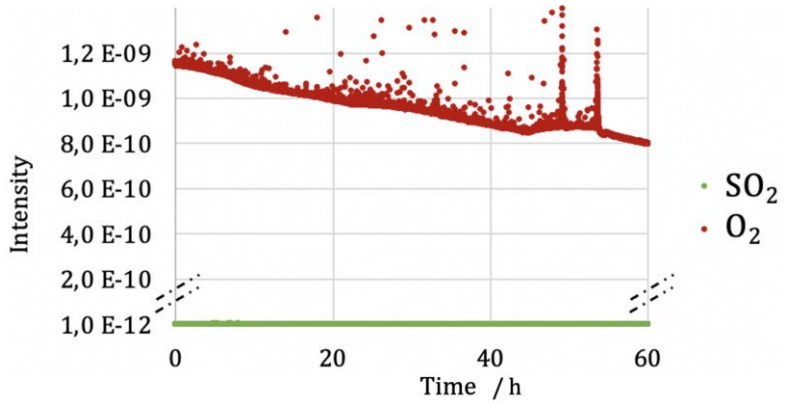

Figure 10: Comparison of O_2 analysis by mass spectrometry during a blistering test of HZC, at 1100°C under pO_2 = 0.2 bar in the semipermeability set-up with the SO_2 blistering of AKM glass in contact with a raw HZC at 1250°C under argon atmosphere.

4.3. Blistering tests

In a previous publication [16] we have demonstrated the feasibility of continuous monitoring of oxygen blistering of HZC refractory at temperature below the monoclinic/tetragonal transformation of zirconia. We have also shown that an incubation period is observed before the beginning of the blistering process. With the set-up described in Section 3.4, at 1100°C, this incubation time can be broken down into two periods: the first one, of around ten hours, corresponds to the oxidation of metallic impurities in the refractory when the refractory is in its pristine state, and a second period which corresponds to the time required (about 1 hour) so that the first bubbles form, rise to the surface of the molten glass and burst. The aim of the following experiments was to compare the behaviour of the HZC refractory below and above the monoclinic-tetragonal transformation and to evaluate the role of the refractory composition on the blistering process.

Influence of temperature

Figures 11 (a) and (b) show the result of the blistering test at 1100°C, below the monoclinic / tetragonal transition. The crucible was an as-made HZC product and, as demonstrated previously [16], an incubation period of ca. 10 h was necessary for totally oxidize the refractory and allow the permeation flux to reach the glass / refractory interface. Moreover, one hour is necessary for the formed bubbles to reach the surface of the molten glass and burst. As shown previously, an intense blistering was observed at 1100°C.

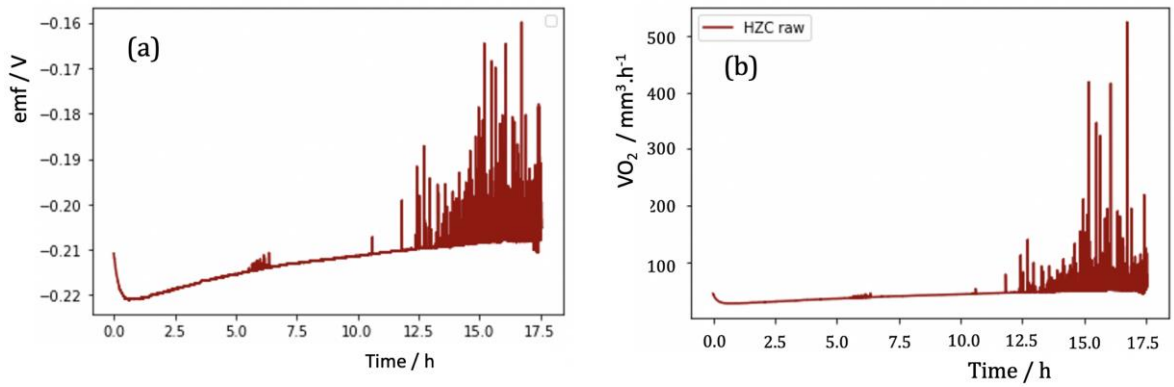

Figure 11: Blistering test of as-made HZC refractory, at 1100°C with AKM glass – pO_2 = 0.2 bar.
(a) variation of the sensor emf downstream the set-up; (b) corresponding oxygen flux in flowing argon.

Then, temperature was raised with a ramp of 100 °C/h followed by a plateau at 1350 °C. As shown in Figures 12 (a) and (b), an intense blistering was observed during ca. 2.5 hour and then stopped. It should be recalled that the time necessary for a bubble to be formed, to rise in the molten glass layer and to burst is of the order of 1 hour. Consequently, according to Figure 12, the blistering phenomenon stopped above the monoclinic/tetragonal transformation.

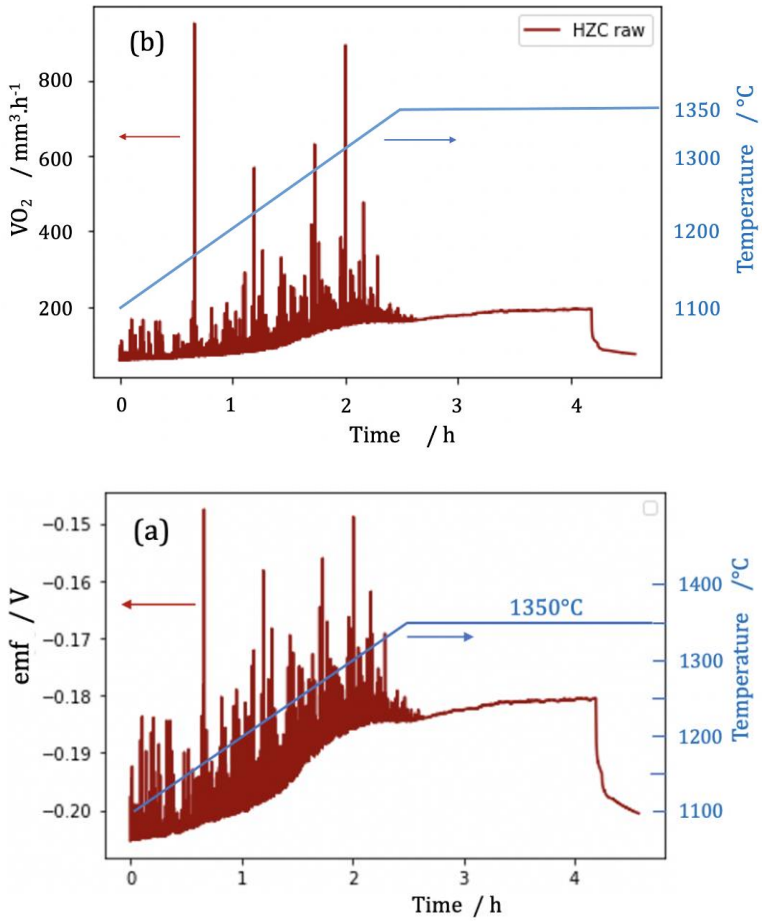

Figure 12: Blistering test during a temperature ramp (100°C/h) from 1100°C to 1350°C, with AKM glass – pO_2 = 0.2 bar. (a): variation of the sensor emf downstream the set-up, (b): corresponding oxygen flux in flowing argon.

This result was confirmed with blistering tests using self-crucibles, below and above the temperature of the monoclinic/tetragonal transformation, at 1100°C and 1350°C, respectively, are shown, Figures 13 (a) and (b).

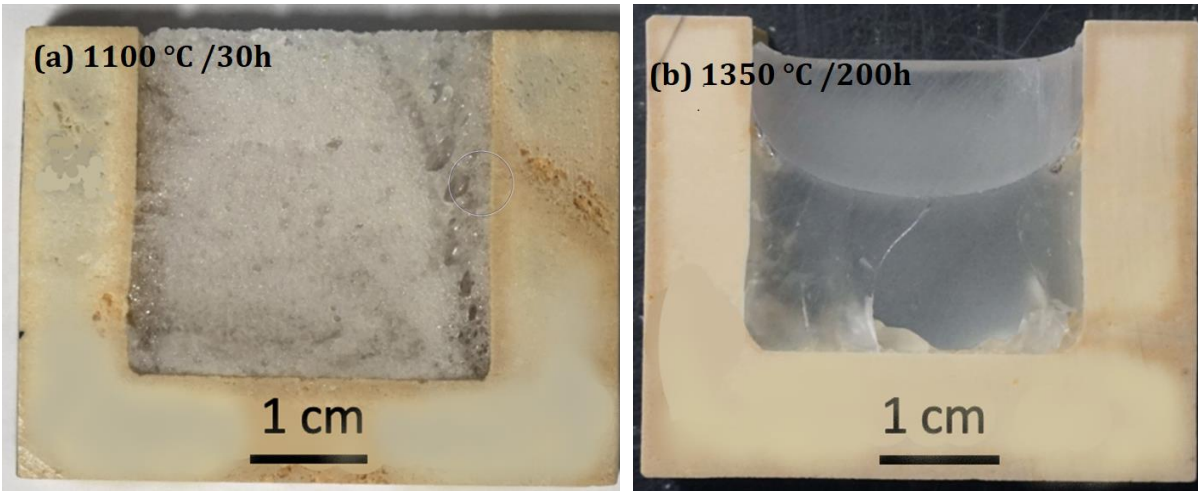

Figure 13: Self-crucible with HZC refractory and AKM glass. (a) 1100°C, 30 h); (b) 1350°C, 200 h)

An intense blistering (foaming) was observed at 1100°C, i.e., many bubbles were observed in the glass phase (see Figure 13 a). On the contrary, at 1350°C, the glass appears transparent with less than 2 bubbles/cm^2 (Figure 13 b). These observations confirm the results obtained with the blistering set-up.

The behaviour of the HZC refractory can be linked to the change of the electrical transport properties at the monoclinic/tetragonal transformation. As recalled in Section 2, the blistering phenomenon can be decomposed in various steps involving bulk diffusion and interface reactions. The overall process can be limited by one step which depends on the experimental conditions. This feature is illustrated in Figure 14. Below the transition temperature, the zirconia phase is monoclinic, and the majority carriers are electronic defects. Consequently, the semipermeation flux is controlled by the minority carriers, i.e., the oxygen vacancies or interstitial oxygen. Above the transition temperature, the zirconia phase becomes tetragonal, with a noticeable increase of the oxygen vacancies mobility and a decrease of the electron holes mobility: the minority carriers become the electronic defects. In both cases, the ambipolar conductivity increases noticeably with temperature with an activation energy of ca. 1 eV. Consequently, in case of blistering process limited by bulk transport, the blistering phenomenon

would increase with temperature. This is the case below the monoclinic/tetragonal transformation of zirconia. As illustrated in Figure 14 (a), the monoclinic zirconia phase being a mixed ionic/electronic conductor, the oxidation process of O^{2-} ions is not the limiting step and the blistering is proportional to the ambipolar conductivity of the refractory. Indeed, it has been demonstrated in solid oxide cells, such as electrolysers, fuel cells, permeation membranes, etc., that the kinetics of electrode reaction of oxygen is very high, provided the electrode material is a mixed ionic electronic conductor [56–58]. The improvement of the oxygen reaction kinetics is due to extension of reaction sites to the whole electrode surface [59–62]. The monoclinic zirconia phase being a mixed ionic-electronic conductor, the surface processes at the glass/refractory interface are not blocking, leading to an intense blistering phenomenon.

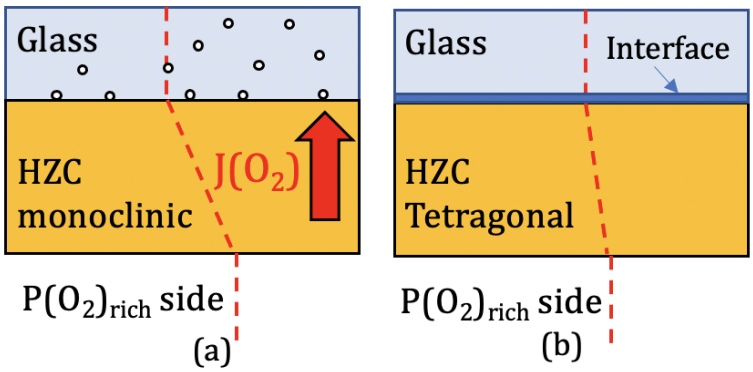

Figure 14: Illustration of the blistering process below (a) and above (b) the monoclinic/tetragonal transformation of zirconia.

However, above the monoclinic/tetragonal transformation, the blistering decreased drastically even if the ambipolar conductivity increases. This feature indicates that the limiting step of the overall process is not the bulk transport but interface processes. As recalled in Section 2, zirconia in a tetragonal phase is mainly an ionic conductor, leading to a poor rate of the surface processes which become limiting. Obviously, the limiting step concerns mainly the oxygen lean side of the refractory. Moreover, the oxygen solubility in molten glass decreases as temperature increases that could increase the sensitivity of the glass/refractory interface to be polarized. If we consider the oxygen electrochemical reaction on an oxide electrolyte with a metallic

electrode, it has been demonstrated experimentally that the polarization phenomenon is higher the lower the solubility of oxygen in the metal: with gold in which oxygen is not soluble, the polarization is very high, in comparison with silver, in which oxygen dissolves easily, which is very little polarized [59, 63]. This feature has been ascribed to the role of delocalization of the oxidation process. In case of very small solubility in the molten glass, the glass/refractory interface can be compared to the Argon/refractory interface for which no oxygen permeation is observed. These two simultaneous phenomena could explain that the oxygen activity at the glass/refractory interface increases up to the oxygen activity of the oxygen-rich side of the refractory. Consequently, the blistering will be very low (see Figure 14 (b)). This result is important industrially because the temperature of glass making furnaces are generally noticeably higher than 1400°C.

Ta_2O_5 doping

With the objective to increase the electrical resistivity of the HZFC products, it has been proposed to dope the zirconia-based refractories with a dopant with a valence higher than 4, such as Nb_2O_5 or Ta_2O_5 [64]. Below the phase transformation, the zirconia phase in HZC is monoclinic and the majority carriers are electron holes under high oxygen pressure. The observed blistering is controlled by the semipermeability flux, proportional to the oxygen vacancy conductivity, which is the minority carrier. As recalled in Section 2, doping with Ta_2O_5, strongly decreases the ionic conductivity of the zirconia phase, suppressing the oxygen semipermeability flux, and then impeding the blistering process. As an example, Figure 15, compares the blistering capacity of HZC and Ta_2O_5 doped HZC refractory (HZX), at 1100°C. No visible peaks are observed with Ta_2O_5-doped refractory, as compared with intense blistering observed with HZC.

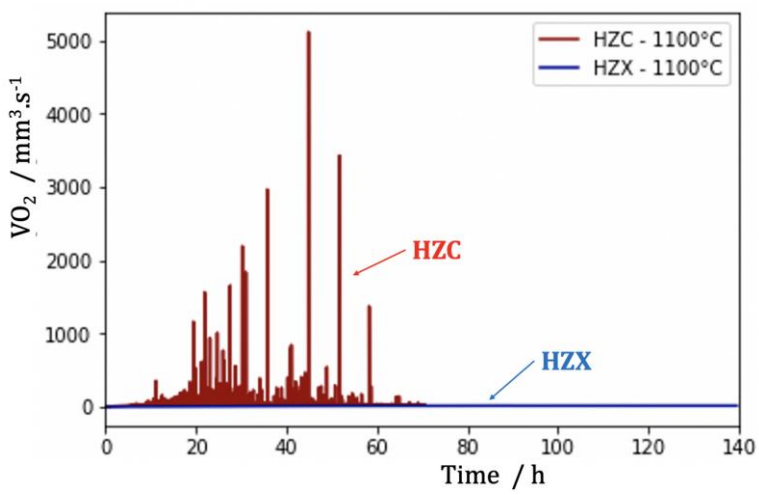

Figure 15: Blistering comparison of HZC and HZX in contact with AKM glass, at 1100°C – pO_2 = 0.2 bar.

5. Conclusion

This work shows that with undoped HZC refractory, the blistering process is observed below the monoclinic/tetragonal transformation of zirconia, and decrease drastically above the transition temperature. The oxygen blistering is linked to the semipermeability phenomenon of zirconia and to the kinetics of the surface processes at the glass/refractory interface. Its intensity depends on the electrical properties of the refractory: in case of mixed ionic-electronic conductivity (monoclinic zirconia), the blistering level is noticeable, while in case of ionic conductivity (tetragonal zirconia) the blistering is very small or even negligible, even if in both cases the ambipolar conductivity increases with temperature. This feature is ascribed to the kinetics of the oxide ions oxidation at the molten glass / refractory interface. It is also shown that appropriate doping of the zirconia phase can suppress the blistering phenomenon. However, with some raw high-zirconia fused cast refractories, especially the most reduced, a temporary blistering phenomenon, with low intensity, ascribed to a redox shock can also be observed.

6. Acknowledgements

Saint-Gobain Research Provence is acknowledged for financial support of this work.

7. References

[1] V. Gottardi, Refractories for the glass industry, J. Non-Cryst. Solids 80 (1-3) (1986) 93–102.

[2] P. Epicoco, B. Coasne, A. Gioia, P. Papet, I. Cabodi, M. Gaubil, Mesoscopic Monte Carlo simulations of microstructure and conductivity of ZrO_2–glass composites, Acta Mat. 61 (2013) 5018–5025.

[3] K. Madi, S. Forest, M. Boussuge, S. Gailliègue, E. Lataste J. Y. Buffiere, D. Bernard, D. Jeulin, Finite element simulations of the deformation of fused-cast refractories based on X-ray computed tomography, Comput. Mater. Sci. 39 (2007) 224–229.

[4] M. Vernerová, L. Němec, J. Kloužek, M. Hujová, Gas release phenomena in soda-lime-silica glass, J. Non-Cryst. Solids 500 (2018) 158–166.

[5] P. Hrma, J. Bartoň, T. L. Tolt, Interaction between solid, liquid and gas during glass batch melting, J. Non-Cryst. Solids 84 (1–3) (1986) 370–380.

[6] J. E. Shelby, Introduction to Glass Science and Technology, Royal Society of Chemistry, Cambridge, UK, 2005.

[7] L. Pilon, A. G. Fedorov, D. Ramkrishna, R. Viskanta, R., Bubble transport in three-dimensional laminar gravity-driven flow – mathematical formulation, J. Non-Cryst. Solids 336 (2) (2004) 71–83.

[8] J. H. Cowan, W. M. Buehl, J. R. Hutchins III, An Electrochemical Theory for Oxygen Reboil, J. Am. Ceram. Soc. 49 (10) (1966) 559–562.

[9] S. Manabe, K. Kitamura, Effect of Sodium Sulfate and Temperature on the Fining of Float Glass, J. Non-Cryst. Solids 80 (1986) 630–636.

[10] F. W. Krämer, Analysis of Gases Evolved by AZS Refractories and by Refractory Glass Melt Reactions – Techniques and Results – Contribution to the Bubble-Forming Mechanism of AZS Material, Glastechnische Ber.-Glass Sci. Technol. 65 (4) (1992) 93–98.

[11] F. A. G. van Dijk, Glass defects originating from glass melt/fused cast AZS refractory interaction, PhD Thesis, Technol. Univ. Eindhoven, 1994. https://doi.org/10.6100/IR417346.

[12] F. G. K. Baucke, G. Röth, Electrochemical mechanism of the oxygen bubble formation at the interface between oxidic melts and zirconium silicate refractories, Glastechnische Ber.-Glass Sci. Technol. 61 (5) (1988) 109–118.

[13] Electrochemistry of Glasses and Glass Melts, Including Glass Electrodes, H. Bach, F.G.K. Baucke, D. Krause, Eds., 2001, Springer Verlag, Berlin.
[14] D. L. Orlov, V. V. Kiryukhin, O. N. Popov, Comparative evaluation of the quality of fuse-cast refractories, Glass Ceram. 43 (1986)148–150.
[15] V. V. Kiryukhin, O. N. Krylova, L. Ya. Levitin, O. N. Popov, Formation of Gaseous Inclusions on the Interface Between Refractory and Glass, Glass Ceram. 45 (1988) 404–407.
[16] J. Hell, P. Vespa, I. Cabodi, O. Citti, F. Fournet-Fayard, J. Fouletier, M. C. Steil, Blistering phenomenon of molten glass in contact with zirconia-based refractories, J. Europ. Ceram. Soc. 41 (2021) 5359–5366.
[17] C. Wang, M. Zinkevich, F. Aldinger, The zirconia-hafnia system: DTA measurements and thermodynamic calculations, J. Am. Ceram. Soc. 89 (12) (2006) 3751–3758.
[18] E. C. Subbarao, Zirconia – an overview, Adv. Ceram., Vol. 3, Science and Technology of Zirconia, A. H. Heuer, L. W. Hobbs, eds., The Am. Ceram. Soc., Inc. Columbus, Ohio, 1981, pp. 1–24.
[19] E. C. Subbarao, H. S. Maiti, K. K. Srivastava, Martensitic transformation in Zirconia, Phys. Status Solidi A 21 (1974) 9–40.
[20] M. Youssef, B. Yildiz, Intrinsic Point Defect Equilibria in Tetragonal ZrO_2 – Density Functional Theory Analysis with Finite Temperature Effects, Phys. Rev. B 86 (2012) 144109.
[21] J. Yang, M. Youssef, B. Yildiz, Oxygen self-diffusion mechanisms in monoclinic ZrO_2 revealed and quantified by density functional theory, random walk analysis, and kinetic Monte Carlo calculations, Phys. Rev. B 97 (2018) 024114.
[22] P. Kofstad, D. J. Ruzicka, Defect Structure of ZrO_2 and HfO_2, J. Electrochem. Soc. 110 (3) (1963) 181–184.
[23] R. W. Vest, N. M. Tallan, W. C. Tripp, Electrical properties and defect structure of zirconia: I, monoclinic phase, J. Am. Ceram. Soc. 47 (12) (1964) 635–640.
[24] R. W. Vest, N. M. Tallan, Electrical properties and defect structure of zirconia: II, Tetragonal Phase and Inversion, J. Am. Ceram. Soc. 48 (9) (1965) 472–475.
[25] P. J. Harrop, J. N. Wanklyn, On the Defect Structure of ZrO_2 and HfO_2, J. Electrochem. Soc. 110 (12) (1963) 1285.
[26] P. Kofstad, Effect of Impurities on the Defects in Oxides and Their Relationship to Oxidation of Metal, Corrosion-Nace 24 (1968) 379–388.
[27] A. Kumar, D. Rajdev, D. L. Douglass, Effect of oxide defect structure on the electrical properties of ZrO_2, J. Am. Ceram. Soc. 55 (9) (1972) 439–445.

[28] S. Deville, G. Guénin, J. Chevalier, Martensitic transformation in zirconia: Part I. Nanometer scale prediction and measurement of transformation induced relief, Acta Mat. 52 (19) (2004) 5697–5707.

[29] O. H. Kwon, C. Jang, J. Lee, H. Y. Jeong, Y-i. Kwon, J. H. Joo, Investigation of the electrical conductivity of sintered monoclinic zirconia (ZrO_2), Ceram. Int. 43 (11) (2017) 8236–8245.

[30] M. M. Nasrallah, D. L Douglass, Ionic and Electronic Conductivity in Y_2O_3-Doped Monoclinic ZrO_2, J. Electrochem. Soc. 121 (2) (1974) 255–262.

[31] A. Guillot, A. M. Anthony, Interpretation of the Electrical Conductivity of ZrO_2 and HfO_2 at High Temperature (1300°C-1600°C) (in Fr.), J. Solid State Chem. 15 (1) (1975) 89–95.

[32] F. Mauvy, J. Fouletier, Determination of thermodynamics and transport properties of non-stoichiometric oxides. Stoichiometry and Materials Science - When Numbers Matter, A. Innocenti and N. Kamarulzaman, Eds., InTech, 2012, Croatia, Chapter 7, pp. 175–202.

[33] J. W. Patterson, E. C. Bogren, R. A. Rapp, Mixed conduction in $Zr_{0.85}Ca_{0.15}O_{1.85}$ and $Th_{0.85}Y_{0.15}O_{1.925}$ solid electrolytes, J. Electrochem. Soc. 114 (7) (1967) 752–758.

[34] J. W. Patterson, Conduction Domains for Solid Electrolytes, J. Electrochem. Soc. 118 (7) (1971) 1033–1039.

[35] H. Tuller, S. Bishop, Point Defects in Oxides: Tailoring Materials Through Defect Engineering, Annu. Rev. Mater. Res. 41 (2011) 369–398.

[36] D. L. Douglass, C. Wagner, Oxidation of Oxygen-Deficient Zirconia and its Relationship to the Oxidation of Zirconium, J. Electrochem. Soc. 113 (7) (1966) 671–76.

[37] A. Madeyski, W. W. Smelzer, Oxygen diffusion in monoclinic zirconia, Mat. Res. Bull. 3 (4) (1968) 369–375.

[38] G. M. Wolten, Diffusionless Phase Transformations in Zirconia and Hafnia, J. Amer. Ceram. Soc. 46 (1963) 418–422.

[39] E. N. S. Muccillo, M. Kleitz, Impedance spectroscopy of Mg-partially stabilized zirconia and cubic phase decomposition, J. Eur. Ceram. Soc. 16 (1996) 453–465.

[40] P. Aldebert, J. P. Traverse, Structure and ionic mobility of Zirconia at High-Temperature, J. Am. Ceram. Soc. 68 (1) (1985) 34–40.

[41] A. Kopp, H. Näfe, W. Weppner, Characterization of the electronic charge carriers in TZP, Solid State Ionics 53-56 (1992) 853–858.

[42] T. K. Gupta, R. B. Grekila, E. C. Subbarao, Electrical conductivity of tetragonal zirconia below the transformation temperature, J. Electrochem. Soc. 128 (4) (1981) 929–931.

[43] J. Chevalier L. Gremillard, A. V. Virkar, D. R. Clarke, The Tetragonal-Monoclinic Transformation in Zirconia: Lessons Learned and Future Trends, J. Am. Ceram. Soc. 92 (9) (2009) 1901–1920.

[44] J. Yang, M. Youssef, B. Yildiz, Oxygen self-diffusion mechanisms in monoclinic ZrO_2 revealed and quantified by density functional theory, random walk analysis, and kinetic Monte Carlo calculations, Phys. Rev. B 97 (2018) 024114.

[45] J. Fouletier, P. Fabry, M. Kleitz, Electrochemical semipermeability and the electrode microsystem in solid oxide electrolyte cells, J. Electrochem. Soc. 123 (2) (1976) 204–213.

[46] S. Kim, Y.L. Yang, A.J. Jacobson, B. Abeles, Oxygen surface exchange in mixed ionic electronic conductor membranes, Solid State Ionics 121 (1999) 31–36.

[47] P. M. Geffroy, A. Vivet, J. Fouletier, N. Richet, P. Del Gallo, T. Chartier, Influence of Oxygen Surface Exchanges on Oxygen Semi-Permeation through $La_{(1-x)}Sr_xFe_{(1-y)}Ga_yO_{(3-\delta)}$ Dense Membrane, J. Electrochem. Soc. 158 (8) (2011) B971–B979.

[48] M.C. Steil, J. Fouletier, P.-M. Geffroy, Surface exchange polarization vs. gas concentration polarization in permeation through mixed ionic-electronic membrane, J. Membr. Sci. 541 (2017) 457–464.

[49] P. Sarrazin, A. Galerie, J. Fouletier, Mechanisms of High Temperature Corrosion: a Kinetic Approach, Trans. Tech. Publ. Ltd, Zürich, Switzerland, 2008.

[50] M. Guillodo, J. Fouletier, L. Dessemond, P. Del Gallo, Oxygen permeation through dense $Bi_2V_{0.9}Cu_{0.1}O_{5.35}$ ceramic membranes, J. Electrochem. Soc. 149 (12) (2002) 93–99.

[50] M. Steil, F. Thevenot, M. Kleitz, Densification of yttria-stabilized zirconia - Impedance spectroscopy analysis, J. Electrochem. Soc. 144 (1) (1997) 390–398.

[51] M. Kleitz, M. Steil, Microstructure blocking effects versus effective medium theories in YSZ. J. Europ. Ceram. Soc. 17 (6) (1997) 819–829.

[52] A. Cordier, H. El Khal, E. Siebert, M. C. Steil, On the role of the pore morphology on the electrical conductivity of porous yttria-stabilized zirconia, J. Europ. Ceram. Soc. 39 (7) (2019) 2518–2525.

[53] L. Pilon, Foams in Glass Manufacturing, in: Foam Engineering: Fundamentals and Applications (ed. P. Stevenson), John Wiley & Sons, Ltd, Chichester, UK, 2012, Chap. 16, pp. 355–408.

[54] F. W. Främer, Solubility of gases in glass melts, Ber. Bunsenges. phys. Chemie 100 (9) (1996) 1512–1514.

[55] H. L. Tuller, Semiconduction and mixed ionic-electronic conduction in nonstoichiometric oxides: impact and control, Solid State Ionics 94 (1997) 63–74.

[56] W. C. Chueh, S. M. Haile, Electrochemistry of Mixed Oxygen Ion and Electron Conducting Electrodes in Solid Electrolyte Cells, Annu. Rev. Chem. Biomol. Eng. 3 (2012) 313–341.

[57] A. Arratibel Plazaola, A. Cruellas Labella, Y. Liu, N. Badiola Porras, D. A. Pacheco Tanaka, M. V. Sint Annaland, F. Gallucci, Mixed Ionic-Electronic Conducting Membranes (MIEC) for Their Application in Membrane Reactors: A Review, Processes 7 (2019) 128.

[58] A. Hammouche, E. Siebert, A. Hammou, M. Kleitz, A. Caneiro, Electrocatalytic Properties and Nonstoichiometry of the High Temperature Air Electrode $La_{1-x}Sr_xMnO_3$, J. Electrochem. Soc. 138 (5) (1991) 1212–1216.

[59] M. Kleitz, T. Kloidt, L. Dessemond, Conventional oxygen electrode reaction: facts and models in: High Temperature Electrochemical Behaviour of Fast Ion and Mixed Conductors, eds. F.W. Poulsen et al. (Riso National Laboratory, Roskilde, Denmark, 1993), pp. 89–116.

[60] M. Kleitz, F. Petitbon, Optimized SOFC electrode microstructure, Solid State Ionics 92 (1996) 65–74.

[61] J. Sunarso, S. Baumann, J. M. Serra, W. A. Meulenberg, S. Liu, Y. S. Lin, J. C. Diniz da Costa, Mixed Ionic – Electronic Conducting (MIEC) ceramic-based membranes for oxygen separation, J. Membr. Sci. 320 (2008) 13–41.

[62] S. P. Jiang, Development of lanthanum strontium cobalt ferrite perovskite electrodes of solid oxide fuel cells – A review, Int. J. Hydrogen Energy 44 (2019) 7448–7493.

[63] R. Jiménez, T. Kloidt, M. Kleitz, Reaction-Zone Expansions and Mechanism of the O_2/Ag/Yttria-Stabilized Zirconia Electrode Reaction, J. Electrochem. Soc. 144 (2) (1997) 582–585.

[64] I. Cabodi, M. Gaubil, Doped refractory with a high zirconia content, US Patent, US8273673B2, 25 Sept. 2012.